

Intercomparison of retrieval codes used for the analysis of high-resolution, ground-based FTIR measurements

F. Hase^{a,*}, J.W. Hannigan^b, M.T. Coffey^b, A. Goldman^c, M. Höpfner^a,
N.B. Jones^d, C.P. Rinsland^e, S.W. Wood^f

^a*IMK-ASF, Forschungszentrum Karlsruhe, Postbach 3640, Karlsruhe 76021, Germany*

^b*Atmospheric Chemistry Division, National Center for Atmospheric Research, P.O. Box 3000, Boulder, CO 80303, USA*

^c*Department of Physics, University of Denver, Denver, CO, USA*

^d*Department of Chemistry, University of Wollongong, Wollongong New South Wales 2522, Australia*

^e*NASA Langley Research Center, Hampton, VA, USA*

^f*National Institute for Water and Atmospheric Research Ltd., Lauder, PB 50061, Central Otago, New Zealand*

Received 7 April 2003; received in revised form 7 November 2003; accepted 17 December 2003

Abstract

A rigorous and systematic intercomparison of codes used for the retrieval of trace gas profiles from high-resolution ground-based solar absorption FTIR measurements is presented for the first time. Spectra were analyzed with the two widely used independent, retrieval codes: SFIT2 and PROFFIT9. Vertical profiles of O₃, HNO₃, HDO, and N₂O were derived from the same set of typical observed spectra. Analysis of O₃ was improved by using updated line parameters. It is shown that profiles and total column amounts are in excellent agreement, when similar constraints are applied, and that the resolution kernel matrices are also consistent. Owing to the limited altitude resolution of ground-based observations, the impact of the constraints on the solution is not negligible. It is shown that the results are also compatible for independently chosen constraints. Perspectives for refined constraints are discussed. It can be concluded that the error budget introduced by the radiative transfer code and the retrieval algorithm on total columns deduced from high-resolution ground-based solar FTIR spectra is below 1%.

© 2004 Elsevier Ltd. All rights reserved.

Keywords: Infrared spectroscopy; Atmospheric trace gases; Radiative transfer; Retrieval algorithms

* Corresponding author. Tel.: +49-7247-82-2434; fax: +49-7247-82-4742.

E-mail addresses: frank.hase@imk.fzk.de (F. Hase), jamesw@nacr.ucar.edu (J.W. Hannigan), coffey@acd.ucar.edu (M.T. Coffey), goldman@acd.ucar.edu (A. Goldman), michael.hoepfner@imk.fzk.de (M. Höpfner), njones@uow.edu.au (N.B. Jones), c.p.rinsland@larc.nasa.gov (C.P. Rinsland), s.wood@niwa.co.nz (S.W. Wood).

1. Introduction

The global network of high-resolution ground-based FTIR spectrometers organized within the framework of the network for the detection of stratospheric change (NDSC) [1–3] provides long-term spectroscopic observations of many trace gases in the terrestrial atmosphere. Some of the stations have already been in operation for several decades. The deduced time series are available via the NDSC database and have been used successfully for trend analysis [4,5] and for the validation of satellite experiments [6]. Various efforts have been taken to assure high data quality and data consistency, e.g. side-by-side intercomparisons [7–9], NDSC gas cells [10,11], and comparisons with other instruments [12] and sondes [13,14]. The side-by-side instrument and total column retrieval intercomparisons are a requirement of the NDSC at primary sites since quantitative comparisons of total column data is a main objective of the NDSC. Retrieval code comparisons have also been performed within the Infra-Red Working Group (IRWG) of the NDSC for the purposes of code validation and consistency of analysis. These included extensive comparisons of total column retrieval algorithms [15] and an initial comparison of profile retrieval algorithms [16].

An important element that is still missing in the algorithm comparisons is a systematic and complete analysis of the error budget for profile data retrieved from these measurements. In this paper, we analyze the impact of different implementations of modeling the atmospheric transmission and especially, of the retrieval algorithms. This includes the errors due to ray tracing, calculation of absorption coefficients, convolution with the instrumental line shape, numerical operations performed in the course of the retrieval, and the a priori information introduced to constrain the solution. In addition, discretization schemes for the continuous atmospheric variables are investigated, including a careful discussion of the different meanings of apparently similar sets of discrete quantities. An optimized discretization scheme for ground-based retrieval work is proposed. In order to achieve a realistic overall error estimation, we compare two completely independent retrieval codes. Both codes, PROFFIT9 and SFIT2 are routinely used for the analysis of FTIR measurements at various NDSC stations.

Here we present results of multiple retrieval tests on a single data set. Since the inversion of trace gas profiles from ground-based measurements is an ill-posed problem, the solution needs to be constrained, and the deduced profile depends on the constraints applied. The constraints apply expected features of the trace gas profile, e.g., the assumed typical variability of a partial column. The results from individual reasonably assumed constraints applied with the respective codes are compared first in a ‘blind’ case. The second more pertinent test of the retrievals is realized when the variability due to the individually chosen a priori assumptions is removed by using equivalent constraints in the ‘matched’ case. These results are further analyzed in greater detail. Empirical functionals of general validity and usefulness for characterizing the compatibility of multiple solutions to ill-posed problems are developed and applied to observational data. Not included here are the errors due to the spectroscopic line parameters data, which have been chosen to be identical, nor due to the assumed Voigt shape of spectral lines, since this assumption is shared by both codes. In the final sections, several areas in the forefront of ground-based profile retrieval analysis are discussed. These are full climatological covariances instead of simplified constraints as has historically been used, restrictions inherent to the use of Gaussian probability functions, and the applicability of positivity constraints. The rigorous intercomparison method presented here can serve as a guideline for future code intercomparisons. In particular, it will enhance the applicability of the results from the

NDSC network of FTIR instruments to validation of many current and future satellite borne remote sensors.

2. Description of the codes SFIT2 and PROFFIT9

2.1. SFIT2

The SFIT2 code has its origin in SFIT1 [17] developed for ground-based retrievals of total column amounts. SFIT1 retrieves total columns of up to five species from nonlinear least-squares fits to individual spectra in a single microwindow by scaling a priori profiles with single multiplicative factors over all layers. Parameters can be included to model instrumental response (e.g., parameters to model a wavelength shift or the variation of the 100% transmission level with wave number). Calculation of absorption coefficients and partition functions employs the algorithm described by Norton and Rinsland [18]. Ray tracing is performed with the FSCATM program [19] with an atmosphere extending from the surface to 100 km. Recent improvements to the ray tracing are included [20].

The program was next modified to allow fitting of multiple spectral intervals simultaneously. This development was largely motivated by the far-infrared work of Carlotti [21], which showed the improved information content achieved when fitting multiple spectral intervals simultaneously. The approach was used for analysis of solar occultation spectra recorded by the ATMOS instrument during its final flight [22]. Fitting remained by nonlinear least squares.

SFIT2 is the extension of SFIT1 to retrieve trace gas profiles which was developed jointly by C. Rinsland of NASA Langley and B. Connor of NIWA Lauder, NZ. The forward model developed for the ATMOS retrievals was retained along with the FSCATM ray-tracing algorithm. The nonlinear least-squares algorithm was replaced with the optimal estimation algorithm used previously primarily for microwave remote sensing. The formalism of Rodgers [23] is assumed, with modifications based on a semi-empirical implementation [24,25]. This incorporates a climatological covariance by specifying an assumed percentage variability of the a priori profile for each layer and a correlation length which is defined as an exponentially decaying intercorrelation between layers. The constraints imposed on the solution are weighted relative to the expected variance of the fit by specifying an assumed SNR value of the measurement, which is an input variable of SFIT2. The SFIT2 algorithm has been used in many previous analyses of ground-based high-resolution spectra [26–31].

2.2. PROFFIT9

The PROFFIT code was developed by Hase (latest software version is 9.0) [32]. The code is available as Windows-executable program. The Rodgers optimal estimation technique is used. The code is capable of handling general covariance matrices. For the efficient construction of simplified empirical covariances, the formalism described by Tikhonov and Phillips [33,34] is used, enabling the user to apply height-dependent constraints on the variability and the first derivative of the profile with respect to height in each layer. The code also allows the application of a positivity constraint on a selected profile in the retrieval vector. This is implemented by performing the inversion on the logarithms of volume mixing ratios (VMRs). This option forces a narrowing of the solution space

to physically meaningful positive VMRs. Minor interfering absorption features from other species can be fitted out by scaling the VMR profiles. The software also allows scaling of only certain altitude intervals of a profile, minimizing bias of estimations of partial columns for weak absorbers with dominant variability in certain altitude ranges, e.g., ClO. PROFFIT9 does not employ a fixed a priori SNR value of the observed spectrum, it takes this information from the residuals of the fit itself, performing an automatic compensation of quality variations in the measured spectra.

The radiative transfer code incorporated into PROFFIT9 is KOPRA [35–37]. KOPRA has been developed for the analysis of MIPAS-Envisat limb sounder spectra. It has been compared extensively with reference codes [38,39]. PROFFIT9 uses KOPRA's ray-tracing algorithm for the calculation of pathlengths and number of molecules in each layer, which uses a newly developed method that circumvents the difficulties inherent to algorithms using Snell's law [40].

3. Setup of the intercomparison

For the purpose of this intercomparison, spectra representing the typical quality of routine NDSC-FTIR measurements have been selected. The spectra are described in detail in Section 3.1 below. The investigated species have been selected to cover a wide variety of species suitable for profile retrieval work. O₃ and HNO₃ have been chosen to represent stratospheric species, i.e., species with VMRs peaking in the stratosphere. The spectral signatures of O₃ used are single lines distinct from interfering features but overlap with their own line wings. The spectral signatures of HNO₃ are complex and comparatively weak, and the capability of the codes to model channel spectra has been tested on this species. HDO and N₂O have been chosen to represent tropospheric species. HDO allows the study of the effects of a strong decrease of VMR with increasing altitude on the retrievals, e.g., the total column depends critically on the lowest part of the retrieved profile. Moreover, HDO is extremely variable. Consequences of this high variability are investigated in Section 6.1 below. N₂O has been included to represent a species well mixed throughout the troposphere, providing the opportunity to compare the application of strong inter-layer correlations in the tropospheric VMR profile between the retrieval codes.

3.1. Spectra and auxiliary quantities

The intercomparison has been performed on a typical set of measured spectra. Table 1 summarizes the characteristics of the three measurements that have been chosen. The spectra have been recorded at two high-latitude NDSC sites with commercial spectrometers. All spectra were approximately calibrated to absolute radiance units by normalizing to blackbody or global source measurements, and were interpolated to a spectral gridwidth of $1/(2 \times \text{maximal optical path difference})$, to avoid unnecessary computational effort in the analysis and to provide a diagonal noise covariance matrix. The spectra are not numerically apodized.

The temperature and pressure profiles have been taken from US National Centers for Environmental Prediction (NCEP) analyses [41]. For altitudes above 45 km, the profile was merged with a CIRA86 [42] monthly climatological mean. The calculation of the refracted solar angle was separately performed by each code. The agreement is within 0.01°.

Table 1
Characteristics of measured spectra

	Spectrum A	Spectrum B	Spectrum C
Location	Thule (76.5 N, 68.7 W, 225 masl)	Kiruna (67.8 N, 20.4 E, 420 masl)	Kiruna (67.8 N, 20.4 E, 420 masl)
Instrument	Bruker 120M	Bruker 120HR	Bruker 120HR
Date and effective UT time	March 4, 2002 16:46:45	February 22, 2001 11:39:58	March 15, 2002 07:57:00
Eff. apparent solar elevation	7.32°	11.70°	14.10°
Optical path difference (cm)	257	180	180
Field of view (diameter, mrad)	3.86	2.39	1.91
Nominal RMS SNR	600	1000	1000
Detector type	Photoconductive MCT	Photovoltaic InSb	Photovoltaic InSb
Species analyzed	O ₃ , HNO ₃	N ₂ O	HDO

Table 2
The microwindows used for the intercomparison

Target species	Interfering species	Wave number ranges (cm ⁻¹)
O ₃	H ₂ O, CO ₂ , (HNO ₃)	782.56–782.86 788.85–789.37
HNO ₃	H ₂ O, (CO ₂), OCS	868.3–869.59 872.80–874.00
HDO	(CO ₂), CH ₄	2659.00–2661.00 2662.40–2664.20
N ₂ O	H ₂ O, CO ₂ , O ₃ , CH ₄	2481.30–2482.60

In case of O₃, HNO₃, and HDO simultaneous fits in two microwindows were performed. Interfering species in brackets have not been fitted, but were taken into account in the radiative transfer calculation assuming mean climatological profiles.

3.2. Spectral windows (microwindows)

For the analysis, appropriate sections of the spectrum are used. An extensive compilation of microwindows used for ground-based retrievals can be found in [43]. The microwindows used for the intercomparison are listed in Table 2. In addition to the dominating spectral features of the target species, there are also spectral features of other species contained in each window. To compensate for the variability of major interfering species, the assumed climatological profiles are scaled in the fit procedure. All interfering species taken into account in each microwindow by both SFIT2 and PROFFIT9 are also listed in Table 2.

Table 3

The layering scheme used for the intercomparison

0.2,	1.4,	2.6,	3.8,	5.0,	6.2,	7.4,	8.6,	9.8,	11.0,
12.2,	13.4,	14.6,	15.8,	17.0,	18.2,	19.4,	20.6,	21.8,	23.0,
24.2,	25.4,	26.6,	27.8,	29.0,	30.2,	31.4,	32.6,	33.9,	35.4,
37.1,	39.0,	41.1,	43.4,	45.9,	48.9,	52.4,	56.4,	61.4,	67.4,
74.4,	82.4								

Given are the altitudes (km) of the 42 levels where the profiles are sampled, enclosing the 41 layers of the model atmosphere. In the case of the Thule spectrum, the observer is at 225 masl, just above the lowest level. For the case of Kiruna, the observer is located at 420 masl, and the whole scheme is shifted upwards by 200 m for the analysis of Kiruna spectra. See Section 3.4 for further details.

3.3. Spectroscopic data

The spectroscopic data used rely on the HITRAN 2000 database [44,45] with updates available through October 2001. The HITRAN line parameters show very good agreement with the observed spectra, as demonstrated by the spectral fittings presented here. In the case of O₃, the new line parameters data given by Birk and Wagner [46] have been used. These parameters give an improved fit to our observed data in the 780 cm⁻¹ region. Both codes used identical spectroscopic data for the target species as well as the interfering species.

3.4. Discretization of the atmosphere

For the purpose of numerical handling, the relevant continuous functions of altitude (pressure, temperature, and number densities of each species) are modeled on a discrete scale. In general, the layering scheme of the forward model can differ from that of the retrieval code. The sampling used for the retrieval must be chosen appropriately to represent all structures in the a priori and retrieved VMR profiles. The radiative transfer code has to represent well auxiliary profiles of temperature and number densities (determining partial and total column amounts). Since the computational effort is directly connected to the number of layers used, schemes are preferred that fulfill all sampling conditions with the least number of layers.

Equidistant layering schemes yield too many layers at high altitudes where the impact on the spectrum, the sensitivity of the retrieval and subsequent retrieved columns is negligible. Layering schemes with equal partial columns in each layer lead to very coarse sampling at high altitudes on the geometrical scale if the total number of layers is not to be too excessive. It is also desirable to avoid large changes in consecutive layer thickness which complicate the setup of climatological covariances. An optimized empirical scheme starts with equidistant and densely spaced levels at the ground (~ 1 km), and above the mid-stratosphere gradually changes to layer thicknesses on the order of the scale height at the top of the model atmosphere.

For this intercomparison the layering scheme typically used in PROFFIT9 has been adopted. The 42 altitude levels listed in Table 3 are for the Thule spectrum (Table 1, A), observed at 225 masl. These values were shifted upwards by 200 m for the analysis of the Kiruna spectra where the observations are made at 420 masl. Although the layer boundaries may be the same, there is an

important difference in interpreting the discrete atmospheric quantities in both codes. Each layer of the input model atmosphere to SFIT2 as computed by FSCATM is defined by a lower altitude boundary and thickness, number density, mass weighted pressure and temperature and mean VMR for all included species. This scheme results in one less layer data point than the level-based PROFFIT9 model given the same input altitude grid. PROFFIT9 performs the retrieval on the level values directly and assumes linear interpolation of the VMR profile and logarithmic interpolation of the number density of air molecules between the levels. To match the vertical grids as close as possible, the SFIT2 layering has been chosen in such a way, that the midpoint of each layer coincides with a PROFFIT9 level. This necessitates a new boundary mid-way from the observer to the first PROFFIT9 level which has the desirable effect of equalizing the number of points in the altitude vectors of each code. For the lowermost point of the profile, an altitude offset of a quarter of the layer thickness (300 m) is inevitable between the retrieved values. When needed, the lowermost point of the SFIT2 profile has been extrapolated to the lowermost PROFFIT9 level by linear extrapolation. Owing to the different interpretations of the discrete atmosphere inherent to the codes, the resolution kernel matrices (see Section 4) are also not fully equivalent. A derivative of the spectrum with respect to a component of the retrieval vector implies the assumption of a rectangular disturbance in the VMR profile for SFIT2, whereas for PROFFIT9, the disturbance is of triangular shape.

To confirm that the chosen layering scheme is appropriate, the total columns have also been determined from the retrieved VMR profiles interpolated to a finer grid in accordance with the implicit assumptions inherent to each code. In the case of PROFFIT9, 83 levels have been used by introducing one additional level mid-way between each pair of the 42 levels specified according to Table 3. The p - T profiles have also been interpolated to the fine grid scheme, assuming linear interpolation in T and $\log(p)$. In the case of SFIT2, a new ray-tracing calculation was performed onto an altitude grid constructed similarly as above. The same forward models as for the original retrievals were used to determine the total columns of the interpolated VMR profiles. For all investigated species, the total columns are practically unchanged from those retrieved using the 42-level grid as shown in Table 4. A second condition to be fulfilled is that the vertical resolution offered by the measurement must not be corrupted by the chosen discretization. This is equivalent to the requirement that the resolution kernel matrix (see Section 4.1, Eq. (3)) must not contain any undersampled structures. It is found that, by far, the narrowest structures emerge in the case of HDO profiles near ground, where the half-width reaches the order of the level spacing. Therefore, we conclude that the chosen discretization is appropriate for general purposes. In the special case of HDO (and probably also H₂O) a slight improvement in vertical resolution near ground might be achievable by choosing a denser level spacing in the lowest troposphere.

4. Quantitative intercomparison of retrieved trace gas profiles

In this section, we introduce a procedure for evaluating the consistency of retrievals from the same measurement. A primary data product of ground-based solar absorption measurements is the total column derived from a spectral absorption feature by the retrieval code. The total columns deduced by each code from the same measurements will be compared for all investigated species. A complete evaluation of the results must also encompass differences in the profile shapes as well as the resolution kernel matrices, which specify the altitude sensitivity and resolution of the results. In Section 4.1, we

Table 4

Overview over retrieved total columns (m^{-2}) for all runs. ‘Fine’ denotes retrievals performed on the subdivided layering scheme. HDO columns are given in terms of total H_2O assuming the HITRAN isotopic abundancies

Species and run	Column SFIT2	Column PROFFIT9	Difference% (SFIT2 – PROFFIT9)
O_3 , blind	$1.481\text{E} + 23$	$1.515\text{E} + 23$	–2.30
O_3 , matched	$1.481\text{E} + 23$	$1.473\text{E} + 23$	+0.54
O_3 , matched, fine	$1.481\text{E} + 23$	$1.473\text{E} + 23$	+0.54
HNO_3 , blind	$3.355\text{E} + 20$	$3.385\text{E} + 20$	–0.89
HNO_3 , blind, fit of channelling	$3.354\text{E} + 20$	$3.377\text{E} + 20$	–0.69
HNO_3 , matched	$3.318\text{E} + 20$	$3.340\text{E} + 20$	–0.65
HNO_3 , matched, fit of channelling	$3.370\text{E} + 20$	$3.352\text{E} + 20$	+0.54
HNO_3 , matched, fine	$3.316\text{E} + 20$	$3.339\text{E} + 20$	–0.70
HDO, blind	$1.887\text{E} + 26$	$1.887\text{E} + 26$	0.00
HDO, matched	$1.889\text{E} + 26$	$1.887\text{E} + 26$	+0.11
HDO, matched, fine	$1.887\text{E} + 26$	$1.887\text{E} + 26$	0.00
N_2O , blind	$5.746\text{E} + 22$	$5.786\text{E} + 22$	–0.70
N_2O , matched	$5.776\text{E} + 22$	$5.787\text{E} + 22$	–0.19
N_2O , matched, fine	$5.777\text{E} + 22$	$5.789\text{E} + 22$	–0.21

will demonstrate that the intercomparison of two retrieval results is most favorable when identical constraints are chosen, since otherwise the unknown true variability of the atmospheric state enters the evaluation. Therefore, the most promising strategy of code intercomparison is to analyze the differences of ‘matched’ results—results of retrievals applying identical constraints—in a variety of situations. In Sections 4.2 and 4.3, quantitative measures of differences in the profiles and resolution kernel matrices will be constructed. A detailed description of inverse methods can be found in [47].

4.1. Intercomparison of retrievals on the same spectrum using different constraints

The intercomparison of retrieved profiles deduced from the same measurement while applying different constraints strongly resembles the task of investigating the consistency of remotely sounded data by different instruments. The latter kind of intercomparison has been investigated in detail by Rodgers and Connor [48]. The modification of the formalism given there for our purpose is outlined in the following.

The optimal estimation solution vector \mathbf{x} satisfies the equation

$$\mathbf{x} = \mathbf{x}_a + (\mathbf{K}^T \mathbf{K} + \sigma^2 \mathbf{S}_a^{-1})^{-1} \mathbf{K}^T [\mathbf{K}(\mathbf{x}_{\text{true}} - \mathbf{x}_a) + \boldsymbol{\varepsilon}] \quad (1)$$

for the case of a linear problem and uncorrelated spectral white noise of variance σ^2 . The assumed mean climatological state is \mathbf{x}_a , with assumed covariance matrix \mathbf{S}_a . $\boldsymbol{\varepsilon}$ denotes the noise vector realized in the measured spectrum. \mathbf{K} is the Jacobian (called weighting function matrix by some authors), which collects the derivatives of the spectrum with respect to each retrieved variable. The actual state realized during the measurement is \mathbf{x}_{true} . The gain matrix

$$\mathbf{G} = (\mathbf{K}^T \mathbf{K} + \sigma^2 \mathbf{S}_a^{-1})^{-1} \mathbf{K}^T \quad (2)$$

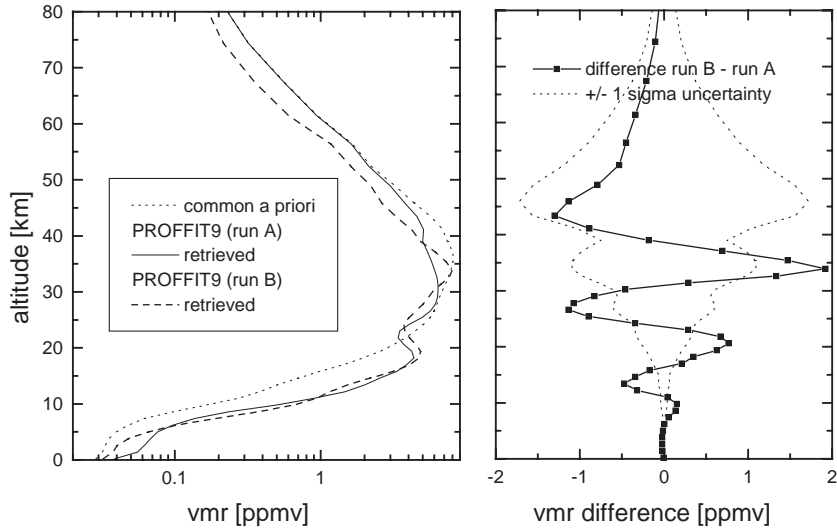


Fig. 1. Left: retrieval results assuming different climatological covariances when analyzing O₃ in the same spectrum. The a priori covariance for run A was the purely diagonal covariance used for the matched run discussed in detail in Section 5.1. The covariance shown in Fig. 19 (right panel) was used as a priori covariance for run B and was also used for S_x in Eq. (5). Right: The one sigma error margins due to estimated atmospheric variability superimposed on the differences of the profiles. More points than expected lie outside the error margins, especially in the troposphere. For details see Section 4.1.

specifies, how each spectral gridpoint affects each component in the solution vector. The resolution kernel matrix (called averaging kernel matrix by some authors)

$$\mathbf{A} = \mathbf{G}\mathbf{K} \tag{3}$$

specifies how the retrieval smears out the fine structure of the difference between the true state and the assumed climatological state $\mathbf{x}_{\text{true}} - \mathbf{x}_a$. With the two sets of retrievals on the same spectrum given, which are fully determined by $\mathbf{x}_1, \mathbf{x}_{a,1}, \mathbf{G}_1, \mathbf{A}_1$ and $\mathbf{x}_2, \mathbf{x}_{a,2}, \mathbf{G}_2, \mathbf{A}_2$, we transform the solutions to a common a priori profile by modifying solution 1 as follows:

$$\tilde{\mathbf{x}}_1 = \mathbf{x}_1 + (1 - \mathbf{A}_1)(\mathbf{x}_{a,2} - \mathbf{x}_{a,1}). \tag{4}$$

Now the covariance $\mathbf{S}_{\Delta x}$ of the difference $\tilde{\mathbf{x}}_1 - \mathbf{x}_2$ can be determined. In contrast to the intercomparison of two instruments with statistically independent noise vectors, the retrievals are applied to the same spectrum with the same noise vector ε . In this case, it follows that

$$\mathbf{S}_{\Delta x} = (\mathbf{A}_2 - \mathbf{A}_1)\mathbf{S}_x(\mathbf{A}_2 - \mathbf{A}_1)^T + (\mathbf{G}_2 - \mathbf{G}_1)\mathbf{D}(\mathbf{G}_2 - \mathbf{G}_1)^T, \tag{5}$$

where \mathbf{D} is a diagonal matrix with $D_{ii} = \sigma^2$. The true climatological covariance \mathbf{S}_x is unknown, as is the difference between the assumed climatological state $\mathbf{x}_{a,2}$ and the true climatological mean. In Eq. (4), we assume that $\mathbf{x}_{a,2}$ represents the true climatological mean reasonably well and neglect the additional term associated with the difference between $\mathbf{x}_{a,2}$ and the true climatological mean in Eq. (5).

Fig. 1 illustrates the method for two PROFFIT9 retrievals of O₃ performed on the same spectrum, but assuming different covariances. The symmetric envelope in Fig. 1 (right panel) overlaid on the

difference in the profiles are the error bars given by $\sqrt{S_{\Delta x, ii}}$. About half of the points lie within the error bar given by the standard deviation, which is less than expected. This is probably due in large part to an underestimated tropospheric variability of the profile, where most points lie outside the quite narrow error margins. A tropospheric variability of about 10% (standard deviation) has been assumed for the true tropospheric variability in Eq. (5), whereas the solutions tend to increase the tropospheric a priori values by about a factor of 2. More sophisticated statistical tests can be performed on the difference between the retrieved profiles, but the inevitable drawback of the strategy is that the atmospheric variability and climatological mean enter the evaluation process, which are poorly known for many species. Although the method is fully appropriate in its original form to compare sounding results of different instruments, it is preferable to focus this intercomparison of the retrieval codes by choosing identical constraints. It can be assumed that codes passing quantitative tests in a variety of situations employing identical constraints on the same spectra are fully consistent.

4.2. Measures of quality for the retrieved profile

In this section, we define measures of quality to quantify the discrepancies between retrievals performed on the same spectrum. These measures should take the quality of the measured spectrum into account, since a higher data quality should lead to better retrievals and hence demands a more accurate analysis procedure. An empirical measure of the currently achievable data quality is the noise level of the measurement. Alternatively, the variance of the fit can be used, given by

$$\sigma^2 = \frac{1}{N} (\mathbf{y}_{\text{meas}} - \mathbf{y}_{\text{fit}})^T (\mathbf{y}_{\text{meas}} - \mathbf{y}_{\text{fit}}). \quad (6)$$

\mathbf{y}_{fit} and \mathbf{y}_{meas} denote the calculated and measured spectra, respectively. N denotes the number of spectral gridpoints. The variance of the fit is typically larger than expected from the instrumental noise level. Given the high SNR achievable in solar absorption measurements, spurious spectral features can be detected in the residuals (see Figs. 4, 8, 12, and 16), which are connected to the imperfect spectroscopic parameters and modelling, errors in the assumed atmospheric temperature stratification, and instrumental imperfections. Thereby, referring to the instrumental noise level leads to a more stringent requirement than referring to the variance of the fit. We will use the pure instrumental noise level.

To construct quantities to be compared with the standard deviation σ we start from the product of the Jacobian and the difference of the VMR profiles $\mathbf{K}_{\text{VMR}}(\mathbf{x}_1 - \mathbf{x}_2)$. \mathbf{K}_{VMR} is the subset of the Jacobian that contains the derivatives with respect to the VMR profile. Since each retrieval incorporates a normalization of the spectra in each microwindow that does not affect the VMR profiles deduced, a further modification of this residual spectrum is appropriate. The derivative of the spectrum with respect to a scaling factor \mathbf{K}_S is used to minimize the standard deviation of the residual spectrum \mathbf{d} :

$$\mathbf{d} = \mathbf{K}_{\text{VMR}}(\mathbf{x}_1 - \mathbf{x}_2) - \mathbf{K}_S(\mathbf{K}_S^T \mathbf{K}_S)^{-1} \mathbf{K}_S^T \mathbf{K}_{\text{VMR}}(\mathbf{x}_1 - \mathbf{x}_2). \quad (7)$$

The quantity Q , defined as the standard deviation of \mathbf{d} divided by the noise level achievable in practice, is a useful empirical estimate of the consistency of the retrievals. If Q is of order unity, the

agreement of both retrievals is considered satisfactory, because the impact of the difference $\mathbf{x}_1 - \mathbf{x}_2$ on the spectrum is of the order of, or below, the noise level of the measurement.

The Q test is necessary, but not sufficient. The difference of the profiles could still show oscillations without increasing significantly the residual spectrum as defined by Eq. (7), since the number of linearly independent rows in the Jacobian is much smaller than the number of levels. For this reason, we define a second residual spectrum \mathbf{d}_{abs} according to Eq. (8):

$$\mathbf{d}_{\text{abs}} = \mathbf{K}_{\text{VMR}}(|\mathbf{x}_1 - \mathbf{x}_2|) - \mathbf{K}_{\text{S}}(\mathbf{K}_{\text{S}}^{\text{T}}\mathbf{K}_{\text{S}})^{-1}\mathbf{K}_{\text{S}}^{\text{T}}\mathbf{K}_{\text{VMR}}(|\mathbf{x}_1 - \mathbf{x}_2|). \quad (8)$$

The standard deviation of \mathbf{d}_{abs} divided by the noise level, defines Q_{abs} . Q_{abs} is sensitive to oscillations in the difference of the VMR profiles because the absolute value of the difference $\mathbf{x}_1 - \mathbf{x}_2$ is used in Eq. (8). A Q_{abs} of order unity also indicates satisfactory agreement.

Whereas the intercomparison of retrieval results with identical constraints is straightforward in the sense that identical results are expected, it is not clear what is to be expected if different constraints are applied. Especially, the Q_{abs} criterion will no longer be fulfilled. However, the quantity Q is still useful because constraining the solution properly, should not prohibit a fit with a variance near the minimum value among all solutions allowed (physically reasonable) by the retrieval code. The variance increases markedly only if the solution is overconstrained [49]. Therefore, all pairs of properly constrained solutions should still satisfy the (essential) Q criterion.

4.3. Intercomparison of resolution kernel matrices

Besides the resulting profiles, the resolution kernel matrix given by Eq. (3) is needed for a complete characterization of the retrieval. If a retrieved profile is to be compared with a profile measured in situ the difference between the in situ profile and the climatological mean assumed in the analysis has to be convolved with the resolution kernel matrix. Analogously, if the consistency of co-located remotely sensed profiles is to be examined, the difference in the associated matrices enters the evaluation. Therefore, we include a comparison of these matrices for the matched runs to demonstrate the full compatibility of the results. As for the profiles themselves, we need a measure of quality to decide whether the matrices are compatible given the current quality of measurement and spectral modelling. Since the linearization of the inversion holds only approximately, the derivatives that enter the calculation of the resolution kernel matrix in general depend somewhat on the assumed profile. Especially, derivatives referring to the a priori profile may somewhat differ from derivatives referring to the solution profile. In the following, we refer to resolution kernel matrices that use linearization around the solution profile. These are needed for instance for smoothing profiles from co-located measurements with high vertical resolution, e.g., sondes or LIDAR, to make the vertical resolution of these profiles comparable with the ground-based FTIR profile.

In the ideal case, the resolution kernel matrices in each pair of matched runs, \mathbf{A}_1 and \mathbf{A}_2 should be identical. The errors emerging from the use of either the resolution kernel matrix \mathbf{A}_1 or \mathbf{A}_2 is of the order of

$$\mathbf{S}_{\text{err}} = (\mathbf{A}_1 - \mathbf{A}_2)^{\text{T}}\mathbf{S}_{\text{a}}(\mathbf{A}_1 - \mathbf{A}_2), \quad (9)$$

where \mathbf{S}_{a} is the assumed covariance of the trace gas profile under consideration, and \mathbf{S}_{err} is the covariance of the expected error in the profile. The appearance of a covariance is unavoidable in the evaluation of the resolution kernel matrices, since they mediate the propagation of features from

the actual atmospheric state into the retrieved profile. For simplicity, we will assume the covariances \mathbf{S}_a to be diagonal in the error estimations given below. We will compare the diagonal elements $\sqrt{S_{\text{err } i,i}}$ with the climatological mean profile and with the error bars on the retrieved profile $\sqrt{S_{\text{inv } i,i}}$ associated with the spectral residuals of the fit

$$\mathbf{S}_{\text{inv}} = \sigma^2 \mathbf{G} \mathbf{G}^T. \quad (10)$$

If the errors due to the mismatch of the resolution kernel matrices are on the order of or below the errors according to Eq. (10) in the altitude intervals where the partial columns are significant, then the agreement of the matrices is satisfactory.

5. Results

For each species results of two runs are shown: The first one is ‘blind’, using the standard SFIT2 and PROFFIT9 retrieval procedure. The second run is the ‘matched’ case where equivalent constraints are used (due to differing interpretations of the discrete layering of the model atmosphere inherent to each code the matched constraints are not identical: see Section 3.4. for details). For analyzing O_3 and HNO_3 , spectrum A has been used, whereas HDO has been derived from spectrum C. The N_2O profiles have been derived from spectrum B. Blind runs illustrate the impact of different but reasonable constraints on the retrieved profiles and total columns. The Q and Q_{abs} values for these runs are given. If the codes are compatible, Q should be of order unity or below. Each pair of matched results will also be examined using the Q and Q_{abs} tests and the differences of the resolution kernel matrices will be subject to the test outlined in Section 4.3. If the codes are compatible, both Q and Q_{abs} values should be of order unity or less for the case of matched runs. The differences of the matrices should give rise to uncertainties on the order of, or less than the errors given by Eq. (10).

A comparison of the resulting columns is given in Table 4 and the Q and Q_{abs} values are listed in Table 5. It should be noted that these values as well as the error margins for the differences in the resolution kernel matrices are based on the pure noise level of the measurement (see Section 4.2). It seems unlikely that in the foreseeable future the residuals in the kind of measurements investigated here will be lowered to such an extent that the acceptance margins adopted here become unrealistically large.

5.1. O_3

In Fig. 2, the blind results for O_3 are shown. The SFIT2 results were generated assuming the same uncorrelated percentage variability of the a priori at all levels. The PROFFIT9 results were generated using a constraint on the first derivative of the profile on the log-VMR scale. Owing to the different constraints, the columns differ by 2.3% (Table 4), but the Q value indicates reasonable agreement (Table 5). The matched case was accomplished by repeating the PROFFIT9 analysis but adopting the SFIT2 a priori and constraints from the blind run. In Fig. 3, the results for the matched constraints case are shown. The columns agree within 0.5%, and the Q_{abs} value is markedly reduced. In Fig. 4, the fit to the measured spectrum is shown. The residuals near the line center are partly due to a slight asymmetry of the instrumental line shape, which has been confirmed by laboratory

Table 5
 Q and Q_{abs} values for various pairs of runs

Compared set of results (SFIT2 vs. PROFFIT9)	Q	Q_{abs}
O ₃ blind run	0.83	9.2
O ₃ matched run	0.22	1.4
HNO ₃ blind run	0.46	6.2
HNO ₃ blind run (fit of channelling)	0.48	5.9
HNO ₃ matched run	0.10	0.89
HNO ₃ matched run (fit of channelling)	0.04	1.3
HDO blind run	1.3	15.0
HDO matched run	4.1	4.4
N ₂ O blind run (Rinsland)	0.33	3.3
N ₂ O matched run	0.42	0.57

For the measurement in the MCT detector band containing the O₃ and HNO₃ microwindows, a noise level of 4000 nW/(cm² sterad cm⁻¹) has been assumed. This is about 0.2% of the maximal continuum level in the bandpass (SNR ~ 600). For the measurements in the InSb detector band containing the HDO and N₂O microwindows, a noise level of 13000 nW/(cm² sterad cm⁻¹) has been assumed. This is about 0.1% of the nominal continuum level in the bandpass (SNR ~ 1000).

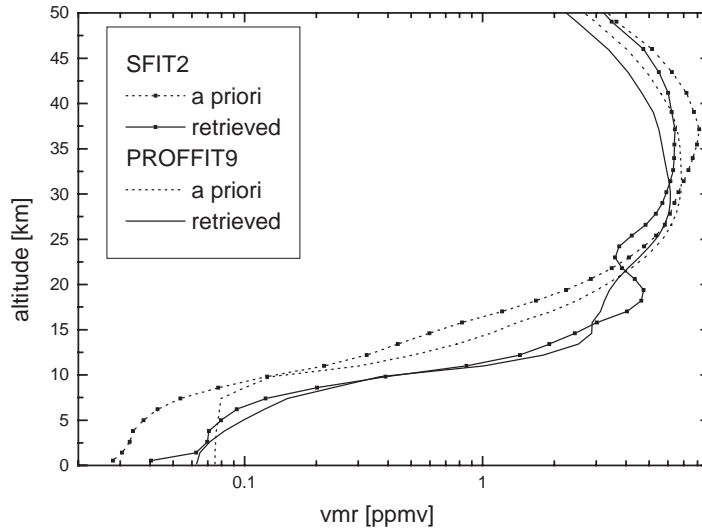
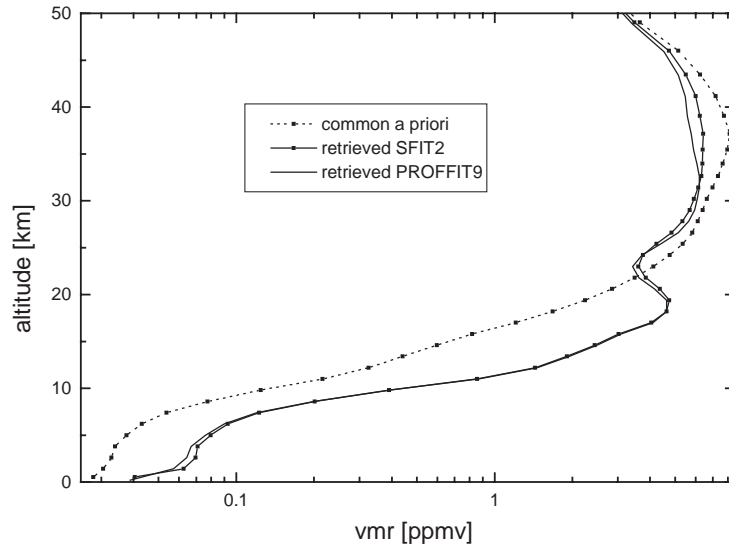
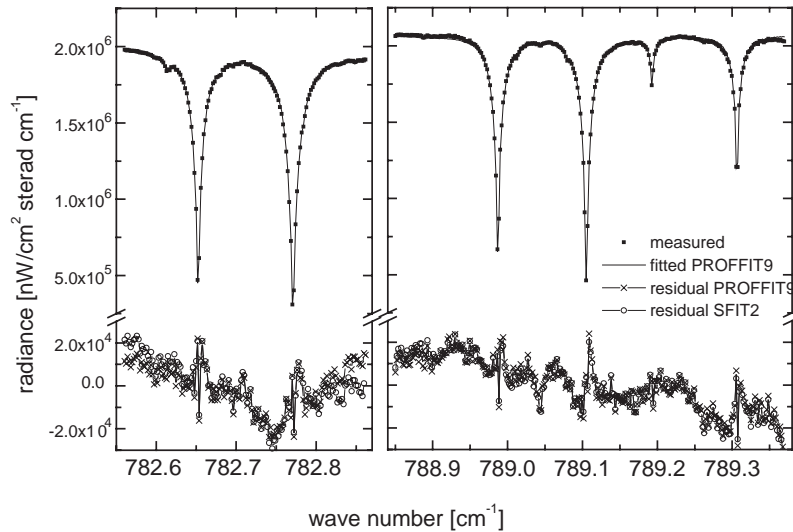


Fig. 2. Retrieved profiles for O₃ blind run.

cell measurements using the same spectrometer, but has not been taken into account here. The low-resolution structures are probably due to far wing effects and minor channelling, that has not been fitted. The residuals of both codes are nearly identical. The agreement between the resolution kernel matrices is also satisfactory (Fig. 5). Near ground level, the noise error margin is exceeded but the absolute value is still much smaller than the climatological mean.

Fig. 3. Retrieved profiles for O_3 matched run.Fig. 4. Fits and residuals for O_3 microwindows, matched run.

5.2. HNO_3

In Fig. 6, the blind results for HNO_3 are shown. The SFIT2 results were generated by applying an altitude-dependent uncorrelated percentage variability of the a priori peaking at 24 km. The PROFIT9 results were generated using a constraint on the first derivative of the profile on the log-VMR scale, and by forcing the profile to the a priori at the lowest and the top levels. Note, that the

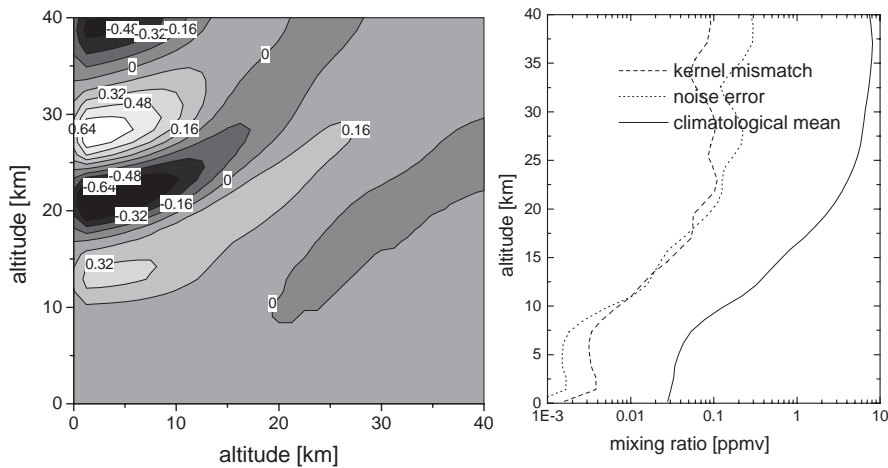


Fig. 5. Left: Resolution kernel matrix for O₃, taken from PROFFIT9, matched run. Right: Kernel mismatch error, a true variability of 20% over the whole altitude range has been assumed.

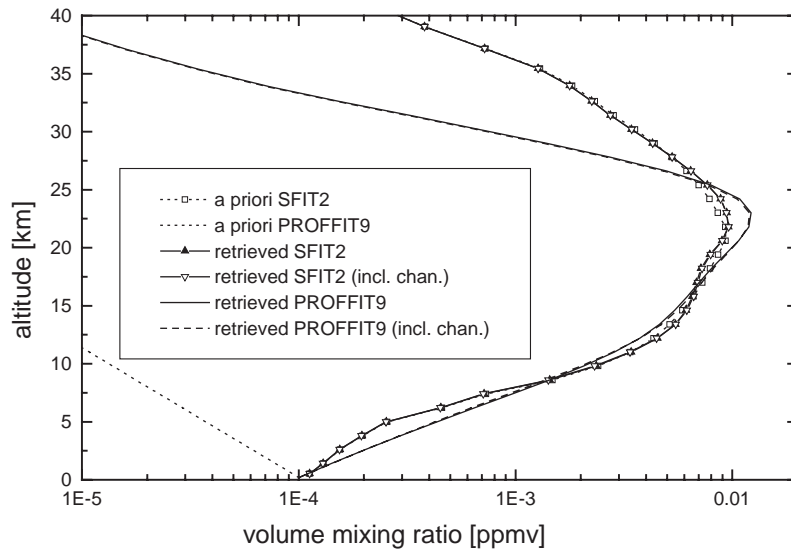


Fig. 6. Retrieved profiles for HNO₃ blind run. (In case of the retrieved profiles marked with ‘incl. chan.’ a fit of channelling with 1.72 cm⁻¹ period has been included.)

PROFFIT9 a priori is simply a straight line on the logarithmic scale assuming a VMR of 1×10^{-4} ppmv at the bottom and a VMR of 4×10^{-9} ppmv at the top of the model atmosphere. In spite of the quite schematic PROFFIT9 constraints, the agreement with the SFIT2 results is remarkably good. A channel spectrum with frequency 1.72 cm⁻¹ and about 1% amplitude has been detected in the residuals. Therefore, the retrievals were also performed including a fit of channelling. The impact of the low-resolution channelling on the retrieved profiles is weak, slightly modifying each profile

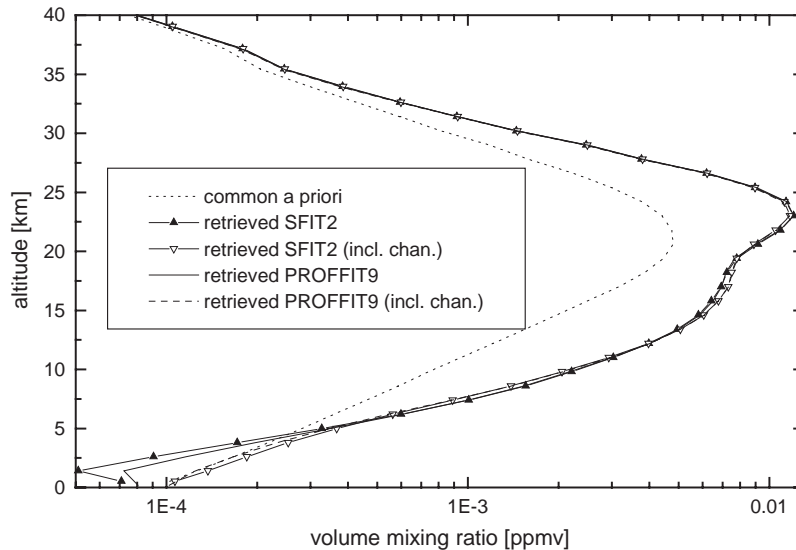


Fig. 7. Profiles for HNO_3 matched run. (In case of the retrieved profiles marked with ‘incl. chan.’ a fit of channelling with 1.72 cm^{-1} period has been included.)

near the ground. The agreement of the columns is better than 1% in both cases (Table 4), and as the Q values indicate the results are compatible (Table 5).

In Fig. 7 the results for matched constraints are shown. For the matched case retrievals from both codes were repeated using the PROFFIT9 a priori and common constraints. The total columns agree well: if channelling is fitted the retrieved total column is increased consistently by 0.3% (Table 4). The Q and Q_{abs} criteria are fulfilled (Table 5). In Fig. 8, the two microwindow fit to the measured spectrum is shown. The low-resolution structures are probably due to far wing effects and some channelling. The residuals of both codes are nearly identical and are markedly reduced, if the channelling is included in the fit. The agreement between the resolution kernel matrices is also satisfactory (Fig. 9). Near ground level, the noise error margin is exceeded but the absolute value of the climatological mean is very small, and the kernel mismatch error is still a fraction of this.

5.3. HDO

In Fig. 10, the blind results for HDO are shown. The SFIT2 results are generated assuming a constant percentage variability down to 12.4 km and then gradually reducing the constraint down to the observation level. The lowest 12.4 km also includes a weak interlayer correlation. The PROFFIT9 results are generated using a constraint on the first derivative of the profile on the log-VMR-scale, and by forcing the profile to the a priori at the highest level. The column values are in very good agreement (Table 4), whereas the Q value slightly exceeds the unity boundary (Table 5). In case of the isotopomer HDO , columns and profiles refer to total H_2O amounts, extrapolated from measured HDO assuming the HITRAN isotopic abundancies. In Fig. 11, the matched HDO results are shown.

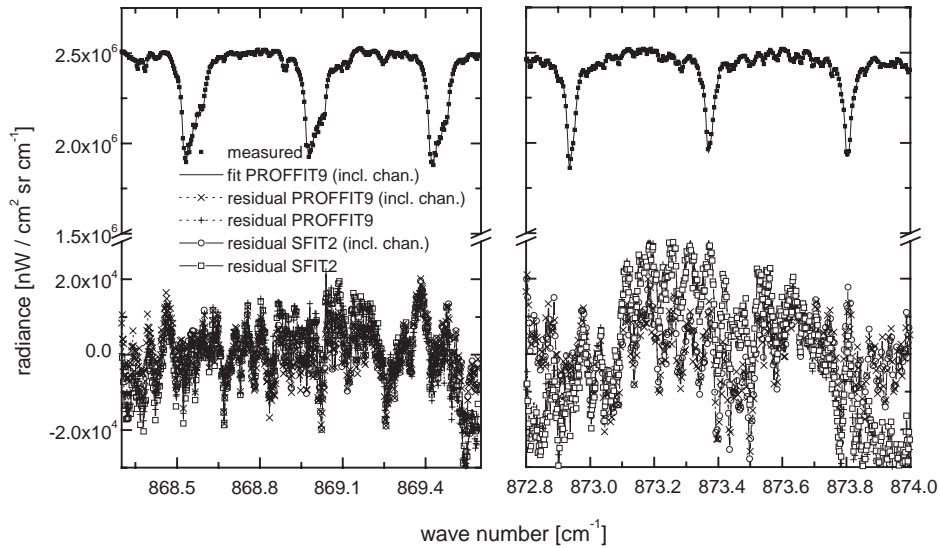


Fig. 8. Fits and residuals for HNO₃ microwindows, matched run.

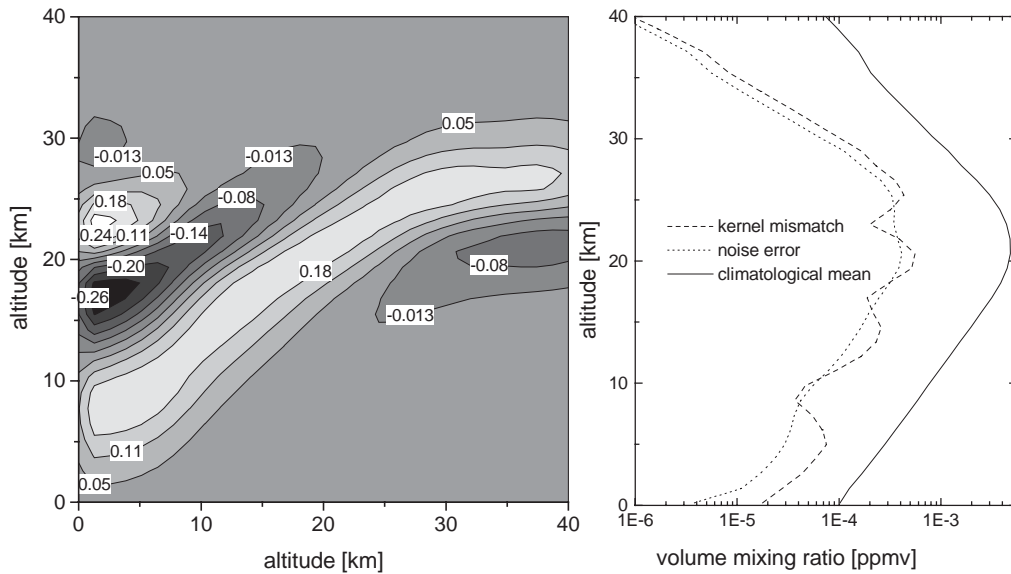


Fig. 9. Left: resolution kernel matrix for HNO₃, taken from PROFFIT9 (matched run without channelling). Right: Kernel mismatch error, a true variability of 20% over the whole altitude range has been assumed.

For the matched run, both the SFIT2 and PROFFIT9 analyses are repeated adopting common constraints. The a priori VMR profile was taken from the PROFFIT9 blind run, and the same value of uncorrelated percentage variability of the a priori over the whole altitude range is used. The Q and Q_{abs} tests are failed (Table 5). In the case of HDO, the extreme gradient in number density

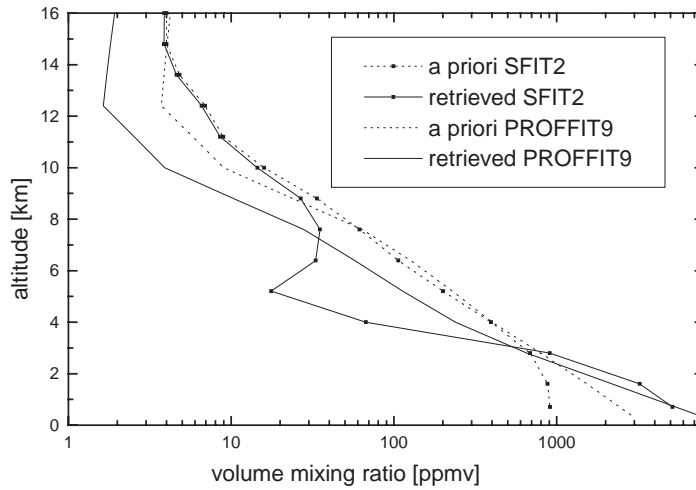


Fig. 10. Retrieved profiles for HDO blind run. The profiles are given in terms of total H_2O assuming the HITRAN isotopic abundancies.

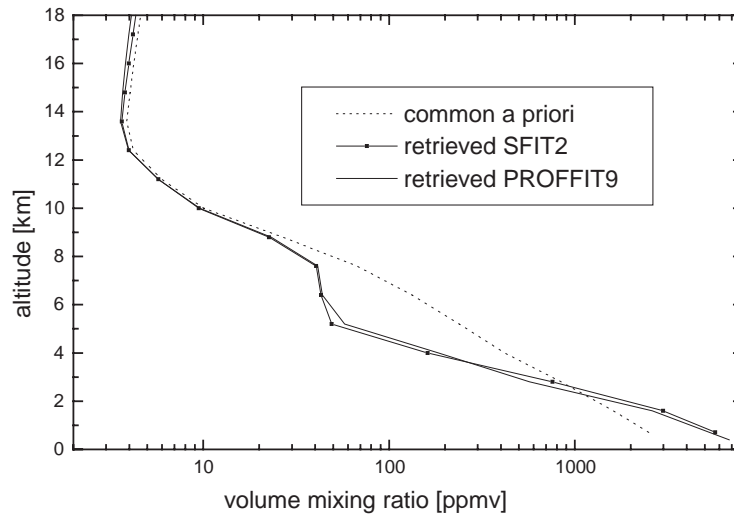


Fig. 11. Retrieved profiles for HDO matched run. The profiles are given in terms of total H_2O assuming the HITRAN isotopic abundancies.

invalidates our layering assumptions (Section 3.4), namely, that the two approaches to the discrete model atmosphere are equivalent. However, since the total columns are in excellent agreement (Table 4), we assume that the results of both codes are nevertheless compatible. Moreover, the residuals which are dominated by spectroscopic errors in HDO and CH_4 are nearly identical (Fig. 12), and the resolution kernel matrices are also consistent (Fig. 13).

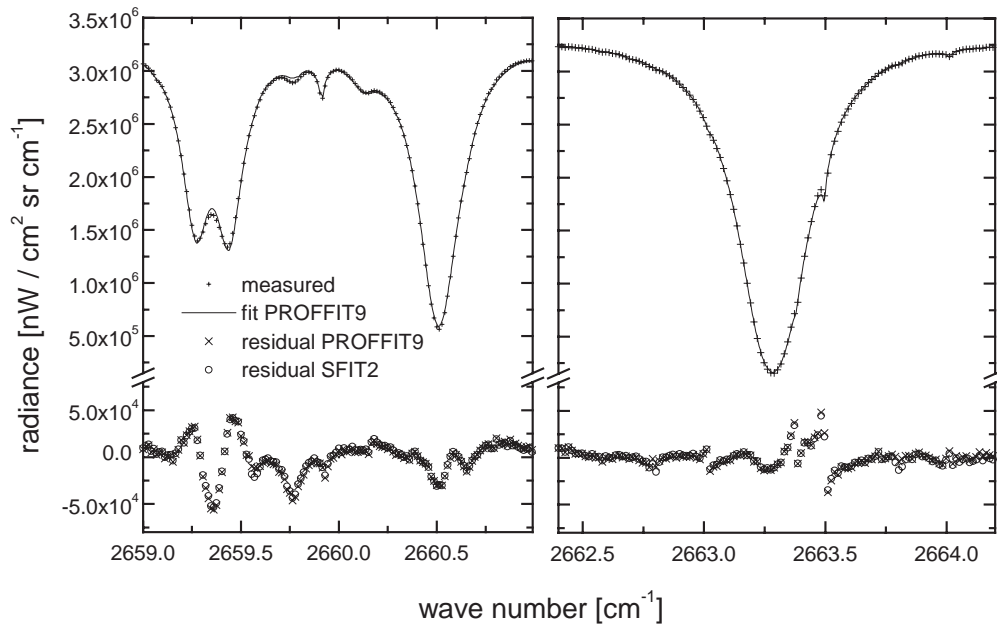


Fig. 12. Fits and residuals for HDO microwindows.

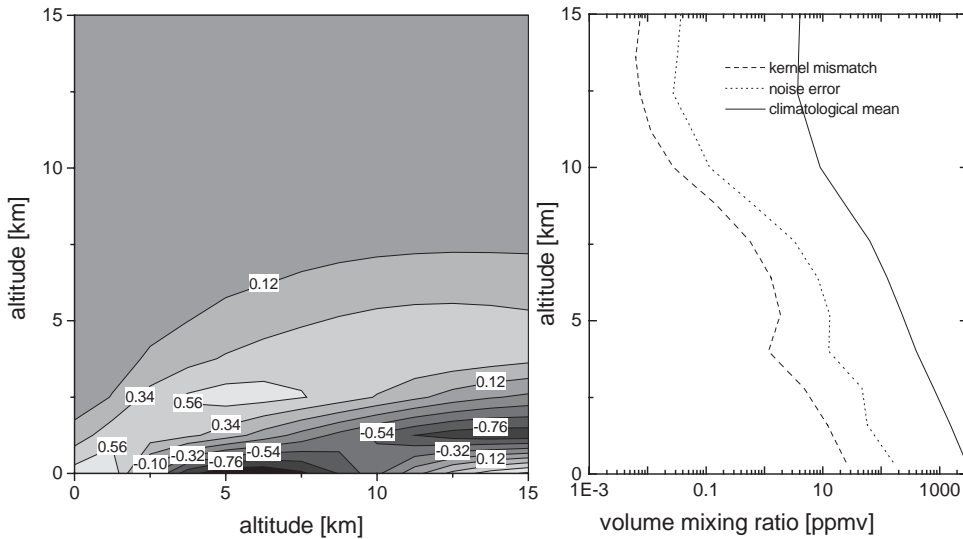


Fig. 13. Left: resolution kernel matrix for HDO, taken from PROFFIT9, matched run. Right: Kernel mismatch error, a true variability of 30% over the whole altitude range has been assumed. The profiles are given in terms of total H₂O assuming the HITRAN isotopic abundancies.

5.4. N₂O

In Fig. 14, the blind results for N₂O are shown. The multiple SFIT2 cases shown were submitted by different users who performed independent retrievals. Whereas all decided to use the same

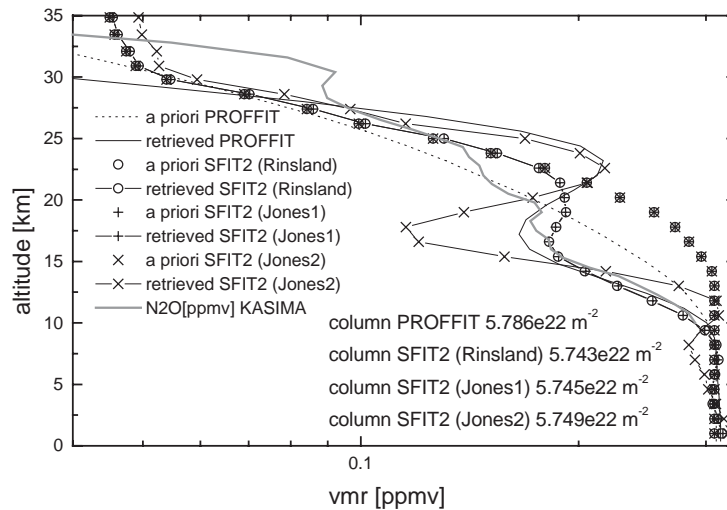


Fig. 14. Retrieved profiles for N_2O blind run.

mid-latitude a priori profile, the climatological covariances were uniquely chosen. Typically, the variability of the a priori increases with altitude and intercorrelations between layers were introduced, to reflect the near constant mixing ratios due to the long lifetime in the troposphere. For the PROFFIT9 retrieval a lowered tropopause height was assumed and a smoothness constraint on the log-VMR scale was applied, which is enhanced over the tropospheric part of the profile. The agreement among the profiles is very good and the total columns agree within 1%. All solutions, especially those with weaker constraints, tend to develop some unusual structures in the stratosphere. For this reason, we have included the N_2O profile predicted by the KASIMA chemical transport model [50,51] in Fig. 14. Indeed, the KASIMA profile agrees very well with the retrieved profiles in the lower atmosphere and shows some structures that may be the seed of the oscillations seen in the retrieved profiles. Since the horizontal resolution of KASIMA is limited ($4^\circ \times 4^\circ$), and the retrieved profiles are convolved with the comparatively poor vertical resolution of the ground-based measurements, a close agreement is not necessarily to be expected.

Fig. 15 shows the N_2O matched results. In contrast to the retrievals for the other species an interlayer correlation extending over the troposphere has been assumed. This generates a covariance with nonzero off-diagonal elements. Both SFIT2 and PROFFIT9 used identical covariances. The profiles agree well with both the Q and Q_{abs} criteria being fulfilled (Table 5), and the columns agreeing to within 0.2% (Table 4). Fig. 16 shows that the fits have nearly identical residuals, and Fig. 17 illustrates the agreement of the resolution kernel matrices.

6. Impact of refined constraints

In the practice of retrieval analysis on ground-based spectra, many investigators use empirical covariances with height-dependent variabilities and exponentially decaying inter-layer intercorrelations. In this section, we demonstrate two possibilities beyond this standard choice of constraints which

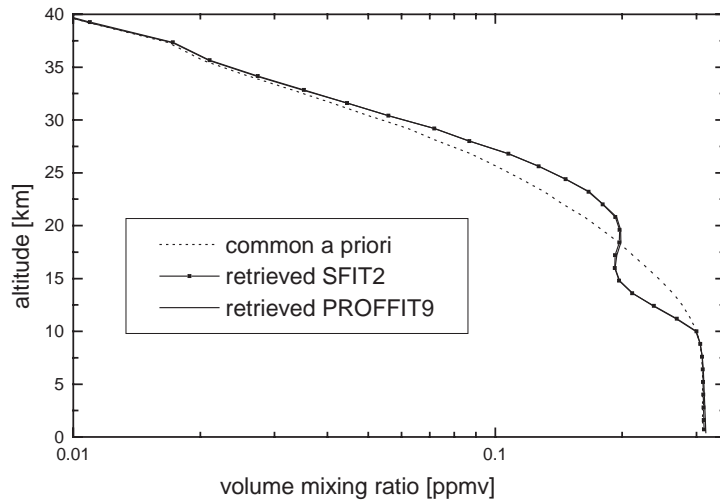


Fig. 15. Retrieved profiles for N₂O matched run.

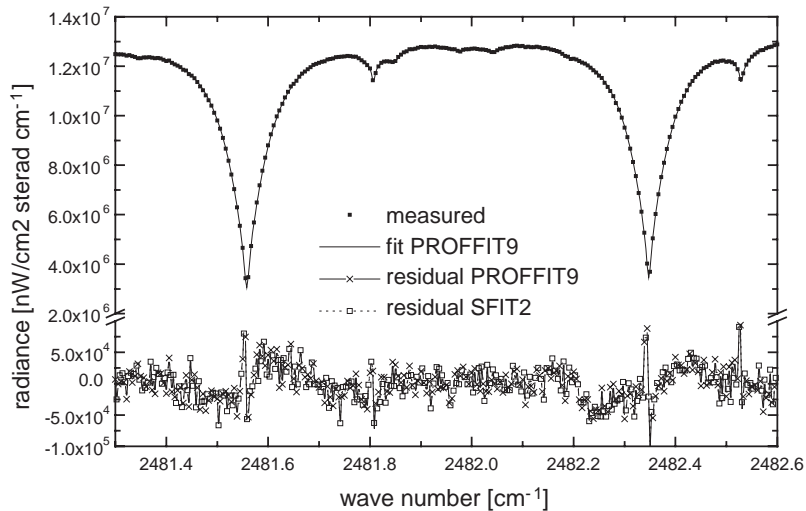


Fig. 16. Fit and residuals for N₂O microwindow, matched run.

also might be combined: the first is the addition of a positivity constraint and the second is the construction and use of refined climatological covariances to properly depict well-known atmospheric processes as variability of tropopause height or down-welling of the stratospheric part of the profile.

6.1. Use of a positivity constraint

We first give some motivation for the log-VMR scale retrieval that has been invoked in the blind runs performed with PROFFIT9. As shown in Table 4, and in Figs. 2, 6, 10, and 14, which display

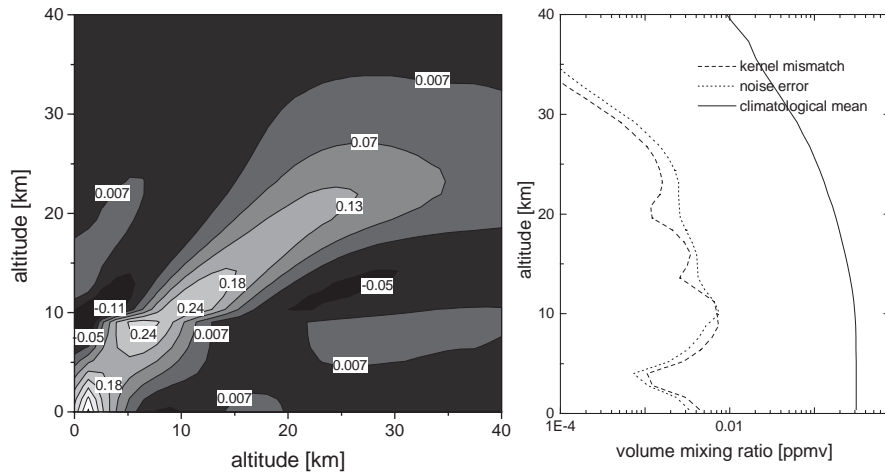


Fig. 17. Left: resolution kernel matrix for N_2O , taken from PROFIT9, matched run. Right: Kernel mismatch error, a true variability of 30% over the whole altitude range has been assumed.

the blind results, the changes introduced by this technique are in general moderate. However, in case of a species with high variability, e.g., HDO, profiles far from the climatological mean do occur in the atmosphere. The classical optimal estimation approach allows for negative VMRs in the retrieved profile. Since the sensitivity to partial columns depends on altitude, the unphysical redistribution of molecular number densities results in perturbed values for the total column.

In the following, we demonstrate this for the unusually dry conditions represented by spectrum B. Assuming the same standard climatological profile and variability as in the matched runs shown in Fig. 11, the retrieved HDO profile shows negative values. If a log-VMR constraint is applied negative values are suppressed, and the total column is decreased by 1.1%. In Fig. 18, left diagram, the profiles retrieved on the log-VMR scale and on the linear scale are shown. The total column is higher in case of the linear retrieval, because the sensitivity peaks between 1.5 and 3.5 km (Fig. 18, right diagram): The negative VMRs are compensated for by increasing the VMR above and below. Since the sensitivity is lower at the compensating altitudes, a larger total column results as compared to a retrieval with positive contributions from all altitudes.

6.2. Use of a climatological covariance

It can be expected that extensive sets of remotely sensed data of stratospheric gases, e.g., from MIPAS, TES, HIRDLS and SCIAMACHY, will be available soon. These observations will also trigger further improvements in chemical transport models (CTMs). As a by-product of this process, reliable climatological information will become available for many species. Improved a priori profiles and covariances will then be available and can be included in the retrieval process of ground-based measurements, minimizing the bias due to the assumed constraints. In this section, we show how to include refined constraints in the analysis and investigate the impact of refined constraints on the retrieval results of the O_3 example.

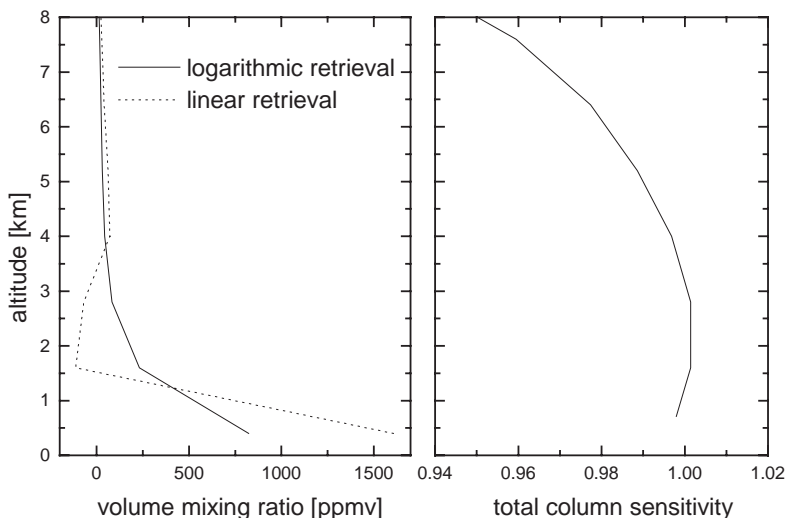


Fig. 18. Left: Retrieved HDO profiles for exceptionally dry conditions (spectrum B, Table 1). The negative VMR value emerging in the case of a linear retrieval are suppressed by performing the inversion on a log-VMR scale. Right: The total column sensitivity of the linear retrieval. The sensitivity peak coincides with the altitudes, where negative VMRs occur. The profiles are given in terms of total H₂O assuming the HITRAN isotopic abundancies.

To generate a refined covariance we define a climatological mean profile of O₃ (identical to the common a priori profile chosen in the section above), and generate a set of profiles by introducing perturbations on this mean profile. The covariance is then deduced from this sample. The perturbations are associated with well-known atmospheric processes. We include a variability of the tropospheric part of the profile, a variability of the stratospheric part, a variability of tropopause height, and a variable down-welling of the stratospheric part of the profile. The deduced covariance is shown in Fig. 19, left diagram. It is quite smooth, since only a small set of parameters acting on large parts of the whole profile was used and shows strong correlations as well as anti-correlations that are not included in the constraints used in Section 5.1 above. We assume that this covariance resembles a covariance that could be derived from a set of profiles taken from a CTM or remotely sensed data, since numerical diffusion effects in both horizontal and vertical directions or constrained retrievals tend to smooth out the fine details of the profiles.

Unfortunately, this covariance cannot be used for the retrieval as is. Since the matrix is constructed from an effectively small set of variable parameters it is, in general, singular. The inverse needed for the retrieval is not available. Performing an eigenvalue decomposition and neglecting the contributions from eigenvectors associated with small eigenvalues allows to provide a modified inverse covariance in a numerically stable manner. However, this modified covariance does not span a fraction of the solution space large enough to stabilize the retrieval.

To stabilize the matrix, and to preserve most of the refined climatological information of the set, additional statistical perturbations at each level are introduced. These perturbations obey a local smoothness condition (Gaussian shaped with a width of a few altitude levels). The modified covariance is shown in Fig. 19, right diagram. It preserves a reasonable portion of the correlations introduced by the physically motivated climatological variables and provides a stable retrieval. The

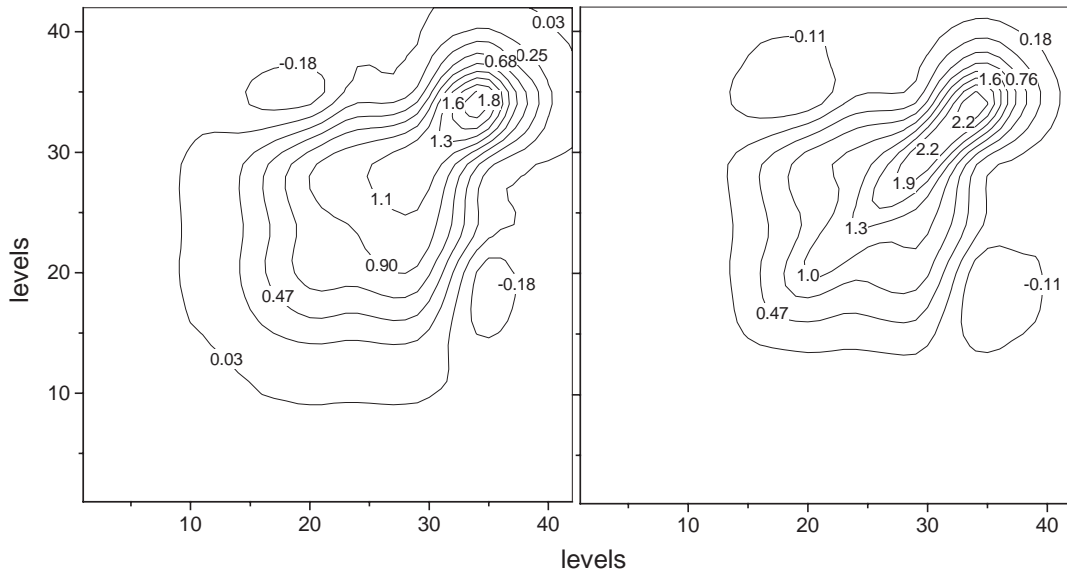


Fig. 19. Left: Original covariance matrix. Right: Modified covariance matrix for inversion.

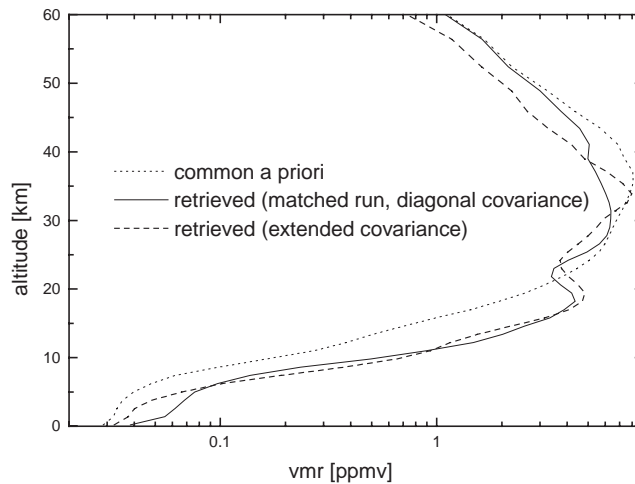


Fig. 20. Retrieved O_3 profile including the modified climatological covariance.

new result is overlaid on the results from the above matched run. The additional information contained in the refined covariance clearly propagates to the solution: the stratospheric part now shows a significant down-welling, while the maximum value of the climatological profile at about 35 km is preserved, and the tropospheric part shows smaller vertical gradients (Fig. 20). The total column is believed to be more accurate, but the change is small (reduction by 0.5%), since over a considerable altitude range the solutions are dominated by the measurement and behave quite similarly.

Nevertheless, over a range of actual observed atmospheric conditions improvements in the results by employing realistic covariances should be expected and this should be more significant in the case of species with less informative spectral signatures than that of O_3 . Of prime importance to the NDSC community is the evaluation of long time series data sets. Here, where a consistent retrieval methodology is highly desired, the use of a realistic climatological covariance to reduce inconsistencies will be beneficial.

7. Conclusions

By investigating retrievals of the species O_3 , HNO_3 , HDO , and N_2O using both SFIT2 and PROFFIT9 we demonstrated the quality and compatibility of the two codes. The initial blind runs with reasonable, independently chosen, constraints indicate that typical column uncertainty budgets for the investigated species can be expected to be on the order of 2% or below. It has been shown in detail in the ‘matched’ cases that profiles and total columns are in excellent agreement when similar constraints are applied. The retrieved profiles are compatible within the typical noise levels currently achieved in high-resolution ground-based solar absorption measurements. The resolution kernel matrices are in reasonable agreement when compared to the errors in the retrieved profiles due to the presence of noise. The columns agree to within 1% or better. SFIT2 and PROFFIT9 have been independently developed with regard to the retrieval codes, ray tracing and radiative transfer algorithms and the smoothing of the calculated irradiated spectrum to match the spectrometer instrument function. Therefore, it can be concluded that the excellent agreement found for the whole set of test retrievals indicates a successful cross-validation of the codes. Moreover, we assume that the remaining minor discrepancies are connected to the various decisions that the code designers have to take in the process of the practical realization of retrieval algorithms in particular, the manner in which atmospheric parameters are discretized. The level of discrepancies indicated by the test runs can serve as a realistic estimation of uncertainty due to the forward modelling and the retrieval procedure.

Further refinements of ground-based retrieval algorithms have been developed and applied to observational data that encompass positivity constraints and the use of full covariance matrices. These refinements yet to be fully explored by the community will likely produce more reliable data time series. In summary, the results of this study enhance the methodology for establishing self-consistency of the NDSC results and its applicability to validation of satellite data.

Acknowledgements

The N_2O profile predicted by the chemical transport model KASIMA has been kindly provided by Dr. R. Ruhnke, IMK-ASF, Karlsruhe, Germany. The work performed at the University of Denver was supported in part by the National Science Foundation and in part by the NASA Upper Atmosphere Research Program. The work performed at NCAR was supported by the National Aeronautics and Space Administration and by the National Science Foundation, which sponsors the National Center for Atmospheric Research.

References

- [1] Kurylo MJ. Network for the detection of stratospheric change (NDSC). *Proc SPIE—Int Soc Opt Eng* 1991;1491: 168–74.
- [2] Kurylo MJ, Zander R. The NDSC—Its status after 10 years of operation. *Proceedings of XIX Quadrennial Ozone Symposium*. Hokkaido University, Sapporo, Japan; 2000. p. 167–8.
- [3] <http://www.ndsc.ws/>.
- [4] Rinsland CP, Zander R, Demoulin P. Ground-based infrared measurements of HNO₃ total column abundances: long-term trend and variability. *J Geophys Res* 1991;96:9379–89.
- [5] Rinsland CP, Mahieu E, Zander R, Jones NB, Chipperfield MP, Goldman A, Anderson J, Russell III JM, Demoulin P, Notholt J, Toon GC, Blavier J-F, Sen B, Sussmann R, Wood SW, Meier A, Griffith DWT, Chiou LS, Murcray FJ, Stephen TM, Hase F, Mikuteit S, Schultz A, Blumenstock T. Long-term trends of inorganic chlorine from ground-based infrared solar spectra: past increases and evidence for stabilization. *J Geophys Res* 2003;108:4252–72.
- [6] Pougatchev NS, Jones NB, Connor BJ, Rinsland CP, Becker E, Coffey MT, Connors VS, Demoulin P, Dzhola AV, Fast H, Grechko EI, Hannigan JW, Koike M, Kondo Y, Mahieu E, Mankin WG, Mittermeier RL, Notholt J, Reichle Jr. HG, Steele LP, Toon GC, Yurganov LN, Zander R, Zhao Y. Ground-based infrared solar spectroscopic measurements of carbon monoxide during 1994 MAPS flights. *J Geophys Res* 1998;103:19,317–25.
- [7] Paton-Walsh C, Bell W, Gardiner T, Swann N, Woods P, Notholt J, Schütt H, Galle B, Arlander W, Mellqvist J. An uncertainty budget for ground-based Fourier transform infrared column measurements of HCl, HF, N₂O, and HNO₃ deduced from results of side-by-side instrument intercomparisons. *J Geophys Res* 1997;102:8867–73.
- [8] Goldman A, Paton-Walsh C, Bell W, Toon GC, Blavier JF, Sen B, Coffey MT, Hannigan JW, Mankin WG. NDSC FTIR intercomparison at table mountain facility. November, 1996. *J Geophys Res* 1999;104:30481–503.
- [9] Griffith DWT, Jones NB, McNamara B, Walsh CP, Bell W, Bernardo C. Intercomparison of NDSC ground-based solar FTIR measurements of atmospheric gases at Lauder, New Zealand. *J Atmos Oceanic Tech* 2003;20:1138–53.
- [10] Coffey MT, Goldman A, Hannigan JW, Mankin WG, Shoenfeld WG, Rinsland CP, Bernardo C, Griffith DWT. Improved vibration-rotation (0-1) H₂O line parameters for validating high resolution infrared atmospheric spectra measurements. *JQSRT* 1998;60:863–7.
- [11] Hase F, Blumenstock T, Paton-Walsh C. Analysis of the instrumental line shape of high-resolution Fourier transform IR spectrometers with gas cell measurements and new retrieval software. *Appl Opt* 1999;38:3417–22.
- [12] Kopp G, Berg H, Blumenstock T, Fischer H, Hase F, Hochschild G, Höpfner M, Kouker W, Reddmann T, Ruhnke R, Raffalski U, Kondo Y. Evolution of ozone and ozone-related species over Kiruna during the SOLVE/THESEO 2000 campaign retrieved from ground-based millimeter-wave and infrared observations. *J Geophys Res* 2002;107:8308–20.
- [13] Pougatchev NS, Connor BJ, Jones NB, Rinsland CP. Validation of ozone profile retrievals from infrared ground-based solar spectra. *Geophys Res Lett* 1996;23:1637–40.
- [14] Schneider M. Continuous observations of atmospheric trace gases by ground-based FTIR spectroscopy at Izana Observatory, Tenerife Island. *Wissenschaftliche Berichte Forschungszentrum Karlsruhe, FZKA 6727*, 2002; ISSN 0947-8620.
- [15] Zander R. IR retrieval algorithms intercomparison for the NDSC, Fourier transform spectroscopy: new methods and applications. *Optical Society Conference*. Santa Fe, New Mexico, USA; February 9–11, 1995.
- [16] Goldman A. Intercomparison of analysis of ground-based IR synthetic spectra. NDSC IR Working Group Meeting, Garmisch, Germany, April 23–25, 1996.
- [17] Rinsland CP, Smith MAH, Rinsland PL, Goldman A, Brault JW, Stokes GM. Ground-based infrared spectroscopic measurements of atmospheric hydrogen cyanide. *J Geophys Res* 1982;87:11,119–25.
- [18] Norton RH, Rinsland CP. ATMOS data processing and science analysis methods. *Appl Opt* 1991;30:389–400.
- [19] Gallery WO, Kneizys FX, Clough SA. Air mass computer program for atmospheric transmittance/radiance calculation: FSCATM. Air Force Geophysics Lab, Bedford, MA, *Environ Res Pap* 1983; 828 (AFGL-TR-83-0065):145p.
- [20] Meier A, Goldman A, Manning PS, Stephen TM, Rinsland CP, Jones NB, Wood SW. Improvements to air mass calculations from ground-based infrared measurements. *JQSRT* 2004;83:109–13.
- [21] Carlotti M. Global-fit approach to the analysis of limb scanning atmospheric measurements. *Appl Opt* 1988;27: 3250–4.

- [22] Rinsland CP, Gunson MR, Wang P, Arduini RF, Baum BA, Minnis P, Goldman A, Abrams MC, Zander R, Mahieu E, Salawitch RJ, Michelsen HA, Irion FW, Newchurch MJ. ATMOS/ATLAS 3 infrared profile measurements of trace gases in the November 1994 tropical and subtropical upper troposphere. *JQSRT* 1998;60:891–901.
- [23] Rodgers CD. Characterization and error analysis of profiles retrieved from remote sounding measurements. *J Geophys Res* 1990;95:5587–95.
- [24] Parrish A, Connor BJ, Tsou JJ, McDermid IS, Chu WG. Ground-based microwave monitoring of stratospheric ozone. *J Geophys Res* 1992;97:2541–6.
- [25] Connor BJ, Parrish A, Tsou JJ, McCormick MP. Error analysis for the ground-based microwave ozone measurements during STOIC. *J Geophys Res* 1995;100:9283–91.
- [26] Pougatchev NS, Connor BJ, Rinsland CP. Infrared measurements of the ozone vertical distribution above Kitt Peak. *J Geophys Res* 1995;100:16,689–97.
- [27] Connor BJ, Jones NB, Wood SW, Keys JG, Rinsland CP, Murcay FJ. Retrieval of HCl and HNO₃ profiles from groundbased FTIR data using SFIT2. Proceedings of XVIII Quadrennial O₃ Symposium, Parco Sci e Technol d'Abruzzo 1996. L'Aquila, Italy, 1996.
- [28] Rinsland CP, Jones NB, Connor BJ, Logan JA, Goldman A, Murcay FJ, Stephen TM, Pougatchev NS, Zander R, Demoulin P, Mahieu E. Northern and southern hemisphere ground-based infrared spectroscopic measurements of tropospheric carbon monoxide and ethane. *J Geophys Res* 1998;103:28,197–218.
- [29] Rinsland CP, Goldman A, Connor BJ, Stephen TM, Jones NB, Wood SW, Murcay FJ, David SJ, Blatherwick RD, Zander R, Mahieu E, Demoulin P. Correlation relationships of stratospheric molecular constituents from high resolution, ground-based infrared solar absorption spectra. *J Geophys Res* 2000;105:14,637–52.
- [30] Rinsland CP, Goldman A, Zander R, Mahieu W. Enhanced tropospheric HCN columns above Kitt Peak during the 1982–1983 and 1990–1998 El Nino warm phases. *JQSRT* 2001;69:3–8.
- [31] Rinsland CP, Meier A, Griffith DWT, Chiou LS. Ground-based measurements of tropospheric CO, C₂H₆ and HCN from Australia at 34°S latitude. *J Geophys Res* 2001;106:20,913–24.
- [32] Hase F. Inversion von Spurengasprofilen aus hochaufgelösten bodengebundenen FTIR-Messungen in absorption. Wissenschaftliche Berichte Forschungszentrum Karlsruhe 2000, FZKA 6512; ISSN 0947-8620.
- [33] Phillips D. A technique for the numerical solution of certain integral equations of the first kind. *J Assoc Comput Math* 1962;9:84–97.
- [34] Tikhonov A. On the solution of incorrectly stated problems and a method of regularisation. *Dokl Acad Nauk SSSR* 1963;151:501.
- [35] Höpfner M, Stiller GP, Kuntz M, Clarmann Tv, Echle G, Funke B, Glatthor N, Hase F, Kemnitzer H, Zorn S. The Karlsruhe optimized and precise radiative transfer algorithm. Part II: Interface to retrieval applications. *SPIE Proc* 1988;3501:186–95.
- [36] Kuntz M, Höpfner M, Stiller GP, Clarmann Tv, Echle G, Funke B, Glatthor N, Hase F, Kemnitzer H, Zorn S. The Karlsruhe optimized and precise radiative transfer algorithm. Part III: ADDLIN and TRANSF algorithms for modeling spectral transmittance and radiance. *SPIE Proc* 1998;3501:247–56.
- [37] Stiller GP, Höpfner M, Kuntz M, Clarmann Tv, Echle G, Fischer H, Funke B, Glatthor N, Hase F, Kemnitzer H, Zorn S. The Karlsruhe optimized and precise radiative transfer algorithm. Part I: Requirements, justification and model error estimation. *SPIE Proc* 1998;3501:257–68.
- [38] Glatthor N, Höpfner M, Stiller GP, Clarmann Tv, Dudhia A, Echle G, Funke B, Hase F. Intercomparison of the KOPRA and the RFM radiative transfer codes. In: Russell JE, editor. Satellite remote sensing of clouds and the atmosphere IV, Proceedings of EOS SPIE, The International Society for Optical Engineering, Florence, Italy. vol. 3867, 1999. p. 348–64.
- [39] Clarmann Tv, Linden A, Funke B, Dudhia A, Edwards DP, López-Puertas M, Kerridge B, Kostsov V, Timofeyev YM. Intercomparison of non-LTE radiative transfer code. In: Smith WL, Timofeyev YM, editors. IRS 2000: current problems in atmospheric radiation. Hampton, VA: A Deepak Publishing; 2001. p. 765–8.
- [40] Hase F, Höpfner M. Atmospheric ray path modeling for radiative transfer algorithms. *Appl Opt* 1999;38:3129–33.
- [41] <http://www.ncep.noaa.gov>.
- [42] Rees D, editor. CIRA 1986. Advances in space research, 1988;8:1–471.
- [43] Meier A, Toon GC, Rinsland CP, Goldman A. A spectroscopic atlas of atmospheric microwindows in the middle infra-red. Publications of the Swedish Institute of Space Physics 1997. IRF preprint 123.

- [44] Rothman LS, Rinsland CP, Goldman A, Massie ST, Edwards DP, Flaud J-M, Perrin A, Camy-Peyret C, Dana V, Mandin J-Y, Schroeder J, McCann A, Gamache RR, Wattson RB, Yoshino K, Chance KV, Jucks KW, Brown LR, Nemtchinov V, Varanasi P. The HITRAN molecular spectroscopic database and HAWKS (HITRAN Atmospheric Workstation): 1996 edition. *JQSRT* 1998;60:665–710.
- [45] Rothman LS, Barbe A, Benner DC, Brown LR, Camy-Peyret C, Carleer MR, Chance KV, Clerbaux C, Dana V, Devi VM, Fayt A, Fischer J, Flaud J-M, Gamache RR, Goldman A, Jacquemart D, Jucks KW, Lafferty WJ, Mandin J-Y, Massie ST, Newnham DA, Perrin A, Rinsland CP, Schroeder J, Smith KM, Smith MAH, Tang K, Toth RA, Vander Auwera J, Varanasi P, Yoshino K. The HITRAN molecular spectroscopic database: Edition of 2000 including updates through 2001. *JQSRT* 2003;82:5–44.
- [46] Wagner G, Birk M, Schreier F, Flaud J-M. Spectroscopic database for ozone in the fundamental spectral regions. *J Geophys Res* 2002; 10.1029/2001JD000818.
- [47] Rodgers CD. Inverse methods for atmospheric sounding: theory and practice. Series on atmospheric, oceanic and planetary physics, vol. 2. India: World Scientific Publishing; 2000.
- [48] Rodgers CD, Connor BJ. Intercomparison of remote sounding instruments. *J Geophys Res* 2003;108:4116–29.
- [49] Hansen PC. Analysis of discrete ill-posed problems by means of the L-curve. *SIAM Rev* 1992;34:561–80.
- [50] Kouker W, Offermann D, Kuell V, Reddmann T, Ruhnke R, Frantzen A. Streamer observed by the CRISTA experiment and the KASIMA model. *J Geophys Res* 1999;104:16405–18.
- [51] Ruhnke R, Kouker W, Reddmann T. The influence of the $\text{OH} + \text{NO}_2 + \text{M}$ reaction on the NO_y partitioning in the Arctic winter 1992/93 as studied with KASIMA. *J Geophys Res* 1999;104:3755–72.